XPS Valence Characterization of Lithium Salts as a Tool to Study Electrode/Electrolyte Interfaces of Li-Ion Batteries

R. Dedryvère,*,† S. Leroy,† H. Martinez,† F. Blanchard,‡ D. Lemordant,‡ and D. Gonbeau†

LCTPCM, Université de Pau, Hélioparc Pau Pyrénées, 2 av. Pierre Angot, 64053 Pau Cedex 9, France, and P.I.M.I.R. (EA 2098), Faculté des Sciences de Tours, Parc de Grandmont, 37000 Tours, France

Received: March 15, 2006; In Final Form: May 18, 2006

X-ray photoelectron valence spectra of lithium salts $LiBF_4$, $LiPF_6$, LiTFSI, and LiBETI have been recorded and analyzed by means of density functional theory (DFT) calculations, with good agreement between experimental and calculated spectra. The results of this study are used to characterize electrode/electrolyte interfaces of graphite negative electrodes in Li-ion batteries using organic carbonate electrolytes containing LiTFSI or LiBETI salts. By a combined X-ray photoelectron spectroscopy (XPS) core peaks/valence analysis, we identify the main constituents of the interface. Differences in the surface layers' composition can be evidenced, depending on whether LiTFSI or LiBETI is used as the lithium salt.

Introduction

Among the components that can be significantly optimized in today's commercial lithium-ion batteries, electrolytes are a key component and constitute a wide field of research.[1] It is now well-known that the cycle life and stability of Li-ion batteries are dependent on the formation of a passivation layer at the graphite negative electrode's surface, usually known as the solid electrolyte interphase (SEI) layer.[2−6] It is generally admitted that the SEI layer originates from the reductive decomposition of the electrolyte solvents and salt on the negative electrode, making up a protective film that prevents side reactions such as solvent cointercalation into graphite and further decomposition of the electrolyte components. However, the formation mechanisms of this layer as well as its composition are not clearly understood and remain a controversial topic, since they play a crucial role in the reversibility of the electrochemical cycling. A thick and resistive SEI film increasing the interfacial impedance is not favorable to battery operation. It is thus very important to optimize solvents (generally a mixture of alkyl carbonate solvents such as dimethyl carbonate (DMC) and ethylene carbonate (EC)), functional additives (such as vinylene carbonate (VC)), and lithium salts to aim at targeted properties of the SEI film.[7−9] Among the various salts that can be used in Li-ion batteries, lithium hexafluorophosphate ($LiPF_6$) is a good compromise between suited physical and chemical properties, such as the dissociation constant in carbonate solvents, ionic mobility, and electrochemical stability, and is therefore the choice lithium salt in today's commercial batteries. However, the disadvantage of $LiPF_6$ lies in its sensitivity to moisture and solvents, and its thermal instabilities that restrict its range of applications. Therefore, other lithium salts are still being investigated as an alternative, especially lithium tetrafluoroborate ($LiBF_4$), lithium bis(trifluoromethanesulfonyl)imide $LiN(SO_2CF_3)_2$ (LiTFSI), and lithium bis(pentafluoroethanesulfonyl)imide $LiN(SO_2C_2F_5)_2$ (LiBETI). Several reported works deal with characterization of electrode/electrolyte interfaces when using either one of these salts.[10−14]

X-ray photoelectron spectroscopy (XPS) is a choice technique to characterize the electrode surfaces of Li-ion batteries.[12,15−18] Interestingly, while XPS core peaks are extensively exploited to identify the species present at the surface, valence spectra are very rarely used in this kind of study. The reason is that experimental valence spectra of electrodes' surfaces after electrochemical cycling are often very difficult to interpret due to the complex mixtures of organic and inorganic species making up the surface layers. However, in previous papers,[19,20] we showed that a careful analysis of valence spectra coupled with a classical core peaks investigation is a powerful experimental tool for a better characterization of electrodes' surfaces.

When trying to characterize electrode/electrolyte interfaces by XPS, small amounts of lithium salt are invariably detected at the surface of the electrode despite washing it by the solvent to remove the electrolyte after electrochemical reaction. The presence of lithium salt can be a handicap for this kind of analysis because all species present at the surface contribute to the valence spectrum. It is thus necessary to know the valence spectra of these lithium salts to be able to interpret electrodes' experimental spectra, which can be rather complex. To our knowledge, no experimental work was reported about the XPS valence spectra of these salts.

In this paper, we report on XPS characterization of $LiPF_6$, $LiBF_4$, LiTFSI, and LiBETI salts by recording their core peaks and valence spectra. We propose a careful analysis of their valence spectra with the help of density functional theory (DFT) calculations, which allow us to simulate them. Then, we use the results of this study to characterize passivation layers forming at the surface of graphite negative electrodes taken from $LiCoO_2$/graphite electrochemical cells using either LiTFSI or LiBETI salt.

Experimental Section

1. Electrochemical Experiments. The graphite negative electrodes, a mixture of synthetic graphite flakes ($d_{50} = 22\ \mu$m) and mesocarbon microbeads (MCMBs, $d_{50} = 10.2\ \mu$m), were kindly provided by SAFT along with positive electrodes ($LiCoO_2$). The active material of the negative electrode was deposited on a Cu foil. For mechanical stability, the graphite

* Corresponding author. E-mail: remi.dedryvere@univ-pau.fr.
† LCTPCM.
‡ P.I.M.I.R.

10.1021/jp061624f CCC: $33.50
Published on Web 06/13/2006

powder was mixed with two binders: styrene butadiene rubber (SBR) and carboxymethyl cellulose (CMC). The electrolyte used was a 1 M LiTFSI (or LiBETI) solution in EC/DEC/DMC (2/2/1) (ethylene-, diethyl-, and dimethyl carbonates). Graphite/$LiCoO_2$ cells were built using Swagelok connectors and cycled with an Arbin battery cycler. Charge was operated in the galvanostatic mode at a C/20 rate with a current density of 177 $\mu A \cdot cm^{-2}$ and stopped at 3.0 or 3.8 V (a C/20 rate corresponds to a current density at which the full capacity of the cell can be charged in 20 h).

For surface studies, the negative electrodes were carefully separated from the rest of the battery components, washed by DMC to remove the electrolyte, and dried prior to being packed into a hermetical sealed glass tube for transportation. All the operation was done in a glovebox under an argon atmosphere.

2. XPS Measurements. To prevent any sample from moisture/air exposure on the analysis site, the XPS spectrometer was directly connected through a transfer chamber to a nitrogen drybox. The samples were removed from their packaging within the drybox and placed onto the sample holder without any contamination. Lithium salts were also grinded in an agate mortar before being placed onto the sample holder.

XPS analyses were carried out with a Kratos Axis Ultra spectrometer using focused monochromatized Al Kα radiation ($h\nu = 1486.6$ eV). The spectrometer was calibrated using the photoemission line Ag $3d_{5/2}$ (binding energy 368.3 eV). For the Ag $3d_{5/2}$ line, the full width at half-maximum (fwhm) was 0.58 eV under the recording conditions. Core peaks and valence spectra were recorded with a 20 eV constant pass energy. The analyzed area of the samples was 300×700 μm^2, and the pressure in the analysis chamber was ca. 5×10^{-7} Pa. Short-time spectra were recorded before and after each experiment and compared to check the nondegradation of the samples in the X-ray beam. The binding energy (BE) scale was calibrated from the hydrocarbon contamination using the C 1s peak at 285.0 eV. Core peaks were analyzed using a nonlinear Shirley-type background,[21] and peak positions and areas were obtained by a weighted least-squares fitting of model curves (70% Gaussian, 30% Lorentzian) to the experimental data. Quantification was performed on the basis of Scofield's relative sensitivity factors.[22] For a more accurate analysis of valence spectra of electrochemically prepared samples, simulated spectra obtained from a weighted fitting of reference compounds' spectra (LiF, Li_2CO_3, CH_3OCO_2Li, LiTFSI, and LiBETI) to the experimental curve were reported. (This concerns only Figures 6 and 7. The other simulated spectra have been calculated by the theoretical method described below.)

Computational Details

Calculations were performed to determine the monoelectronic energy levels of the various salts in order to interpret and simulate their XPS valence spectra using Koopman's theorem approximation. Geometry optimizations were carried out at the DFT/B3LYP[23] level of theory using the Gaussian 98 program[24] and the standard 6-311G* basis set.

The intensities of XPS valence spectra were estimated using the Gelius intensity model,[25−27] which is based on the assumption that the cross section of a molecular orbital (MO) is determined by the cross sections of the corresponding atomic orbitals (AOs). According to this model, the intensity of the *j*th MO is given by the following equation:

$$I_j \propto \left(1 - \frac{3\cos^2\theta - 1}{4}\beta_j\right)\sum_{i\mathrm{AO}} P_{j,i}\sigma_i \qquad (1)$$

where *i* refers to the *i*th AO, θ is the angle between the incoming unpolarized photon direction and the direction of the emitted photoelectrons, β_j is an asymmetry factor ($-1 \le \beta_j \le 2$), $P_{j,i}$ are factors describing the weight of the contribution of the *i*th AO to the MO, and σ_i is the atomic photoionization cross section relating to the *i*th AO.

For each MO, the weighted sum is extended over all of the valence AOs using Scofield's atomic photoionization cross sections.[22] The term ($3\cos^2\theta - 1$) vanishes for the "magic angle" $\theta = 54.74°$. The geometry of the Kratos Axis Ultra spectrometer used in this work corresponds to $\theta = 55°$, so the term containing the molecular asymmetry parameter (β_j) can be neglected. Thus, eq 1 can be simplified as follows:

$$I_j \propto \sum_{i\mathrm{AO}} P_{j,i}\sigma_i \qquad (2)$$

Simulated XPS valence spectra were constructed from the monoelectronic energy levels (ϵ_j) and the intensities (I_j) calculated for each MO. They consist of a series of peaks centered at the monoelectronic energies (ϵ_j). To obtain a simulation closer to the experiment, each peak was represented by a functional shape made up of a combination of Gaussian and Lorentzian profiles (70% Gaussian, 30% Lorentzian). As usual, when using this kind of simulation, the energy scale of the so-obtained spectra was shifted to account for relaxation and correlation effects as well as differences in reference levels.[28,29] Finally, the best fit with the experimental spectrum is obtained after a linear contraction of the BE scale.

Results and Discussion

1. XPS Characterization of Lithium Salts. *Core Peaks.* XPS C 1s, F 1s, Li 1s, B 1s, P 2p, N 1s, S 2p, and O 1s core peaks of lithium salts $LiBF_4$, $LiPF_6$, LiTFSI, and LiBETI have been recorded, and the corresponding values of binding energies (BEs) have been reported in Table 1. For each compound, all 1s core peaks consist of a single peak and 2p core peaks consist of a sole doublet, all assigned to only one type of environment. The BEs of F 1s spectra vary from 687.5 to 688.6 eV, and the BEs of Li 1s spectra vary from 56.6 to 58.2 eV for all salts. The BE of the B 1s core peak is 195.9 eV for $LiBF_4$, and the BE of the P 2p core peak is 138.2 eV for $LiPF_6$. It is worth noting that a shift can be observed between the BEs measured for pure salts, just like here, and the BEs measured for small amounts of lithium salts at electrodes' surfaces. This phenomenon is due to the XPS differential charging effect induced by the presence of insulating species at the surfaces of conducting electrodes. This shift can be rather important to the lower BE, since, for $LiPF_6$, for example, P 2p values of 136.5−137.2 eV and F 1s values of 687.0 eV have been measured at the surface of graphite negative electrodes or $Li(Ni,Co)O_2$ positive electrodes.[18,30]

Concerning LiTFSI and LiBETI salts, the BEs of N 1s and O 1s spectra are 399.6 and 533.0 eV and the BE of the S $2p_{3/2}$ component is 169.4 eV. XPS core peaks of both salts are almost identical except for the C 1s spectrum, for which a sole peak at 293.0 eV can be observed for LiTFSI ($LiN(SO_2CF_3)_2$), assigned to CF_3-like carbon atoms, and two peaks at 291.1 and 293.4 eV can be observed for LiBETI ($LiN(SO_2C_2F_5)_2$), assigned to CF_2-like and CF_3-like carbon atoms, respectively. The C 1s signature of CF_3-like carbon is observed at a slightly higher

TABLE 1: Binding Energies (eV) from XPS Core Peaks of Lithium Salts $LiBF_4$, $LiPF_6$, LiTFSI, and LiBETI

peak	$LiBF_4$	$LiPF_6$	LiTFSI	LiBETI
C 1s				291.1
			293.0	293.4
F 1s	687.5	687.9	688.6	688.6
Li 1s	57.5	58.2	56.6	56.7
B 1s	195.9			
P 2p		138.2		
N 1s			399.6	399.7
S $2p_{3/2}$			169.4	169.5
O 1s			533.0	533.0

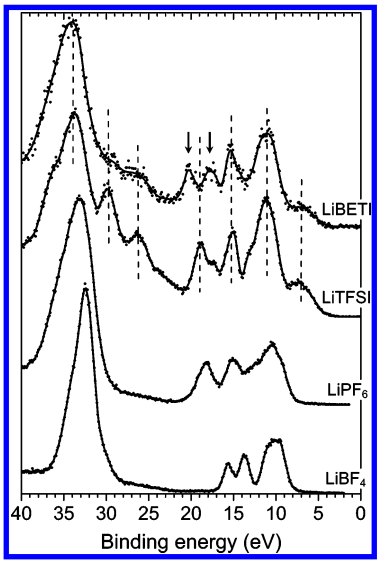

Figure 1. Experimental valence spectra of $LiBF_4$, $LiPF_6$, LiTFSI, and LiBETI.

BE in LiBETI than in LiTFSI due to the presence of two fluorine atoms as second neighbors.

Experimental Valence Spectra. Figure 1 shows the experimental XPS valence spectra of the same samples. The spectrum of $LiBF_4$ consists of a narrow and high peak at 32−33 eV, two small peaks at 15.6 and 13.7 eV, and a massif at 9−11 eV. The assignment of each component of all spectra will be detailed below.

The spectrum of $LiPF_6$ resembles that of $LiBF_4$. It consists of a large and broad peak at 32−35 eV, two small peaks at 18.3 and 15.1 eV, and a broad massif with a shoulder at 12−13 eV and a maximum at 10.5 eV.

The spectrum of LiTFSI shows numerous components. It consists of a first large and broad massif with a maximum at 34 eV, two peaks at 30 and 26 eV and a shoulder at 23 eV, and a second massif between 20 and 5 eV including numerous peaks. The spectrum of LiBETI is very close to that of LiTFSI, which was expected considering the similarity in both compounds' chemical formulas. However, we can notice two main differences: (1) a smaller intensity for both peaks at 30 and 26 eV and (2) the appearance of two peaks at 20.3 and 17.8 eV, while the spectrum of LiTFSI consists of a single peak at 18.8 eV with a shoulder at 17.4 eV in that energy region.

2. Calculations and Simulated Spectra. The aim of this computational approach is the interpretation and the simulation of valence spectra of these lithium salts in order to show that each recorded experimental valence spectrum can be completely assigned to a pure salt and not to a mixture of compounds resulting from degradation of the salt in the X-ray beam during XPS experimentation. Indeed, such molecular compounds could be X-ray-sensitive and may partially decompose.

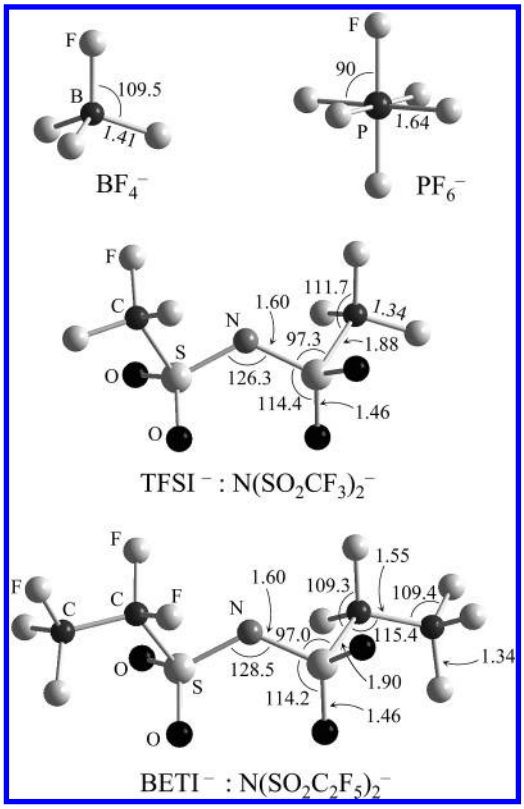

Figure 2. Optimized structures of BF_4^-, PF_6^-, $TFSI^-$, and $BETI^-$ anions by DFT/B3LYP/6-311G* with selected parameters.

For each compound, an optimization of geometrical parameters was carried out at the DFT/B3LYP level of theory. The results obtained for bond distances and angles are reported in Figure 2. As a very low contribution of lithium atoms to the valence spectrum is expected, due to the low contribution of atomic orbitals (AOs) of Li to the valence molecular orbitals (MOs), for all of the salts, only the corresponding anions have been considered. For $LiBF_4$ and $LiPF_6$, a simple regular tetrahedral BF_4^- anion and a simple regular octahedral PF_6^- anion were considered, respectively. For LiTFSI and LiBETI, $N(SO_2CF_3)_2^-$ and $N(SO_2C_2F_5)_2)^-$ anions with C_2 symmetry were considered for the calculations. According to previous works,[31−34] the C_2 symmetry corresponds to the minimum global energy for both $TFSI^-$ and $BETI^-$ anions. The authors have optimized these geometries using ab initio Hartree−Fock methods to calculate the vibrational frequencies of infrared and Raman spectra of $TFSI^-$ and $BETI^-$ anions. Arnaud et al.[31] showed that the most stable $TFSI^-$ conformer corresponds to a dihedral angle of $d(C-S-S-C) = 94.6°$ but that this angle has a very low influence on the energy and, therefore, the $TFSI^-$ structure is very flexible. In our case, we obtain a dihedral angle of $d(C-S-S-C) = 85.2°$ for $TFSI^-$ and $d(C-S-S-C) = 102.3°$ for $BETI^-$. Moreover, for $BETI^-$, the dihedral angle is $d(C-C-S-N) = 180°$, so that bound atoms C−C−S−N are located in the same plane.

$LiBF_4$ and $LiPF_6$. Using the simple BF_4^- and PF_6^- model anions, the computational method allowed us to assign the different components of the valence spectra of $LiBF_4$ and $LiPF_6$. Figure 3 shows experimental spectra (a) and calculated spectra (b) as defined in the computational details section together with diagrams of MOs corresponding to the different monoelectronic energy levels. Only the dominant characters of the MOs have been illustrated. Degenerated MOs have been indicated by ×2 or ×3.

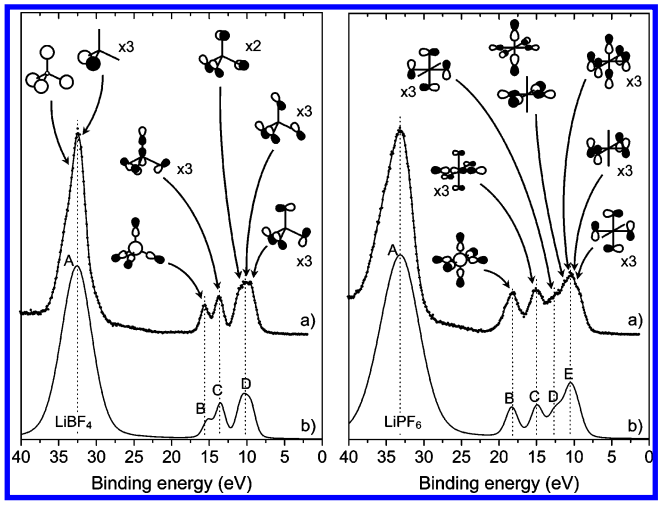

Figure 3. Experimental (a) and calculated (b) valence spectra of $LiBF_4$ and $LiPF_6$, with MOs corresponding to the different energy levels ($\times 2$ and $\times 3$ indicate degenerated MOs).

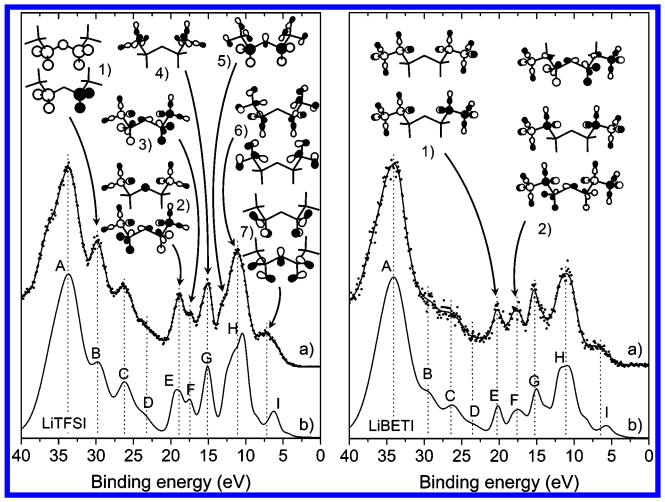

Figure 4. Experimental (a) and calculated (b) valence spectra of LiTFSI and LiBETI, with MOs corresponding to different energy levels (for peaks G−I of LiTFSI, only selected MOs have been represented).

For $LiBF_4$, the calculation results allowed us to assign peak A at 32−33 eV to the photoionization of four MOs of dominant F 2s character. The contributions of boron's AO to these MOs are very low, and thus, peak A has a strong atomic character. Peak B at 15.6 eV can be assigned to the photoionization of one MO with bonding F 2p and B 2s character. Peak C at 13.7 eV corresponds to three degenerated MOs with bonding F 2p and B 2p character. Thus, both peaks B and C are representative of B−F bonds in $LiBF_4$. Finally, the massif at 9−11 eV can be assigned to a nonbonding MO of dominant F 2p character (lone pairs).

For $LiPF_6$, the calculation results allowed us to propose the same kind of interpretation. In the same way as $LiBF_4$, peak A at 32−35 eV can be assigned to six MOs of dominant F 2s character (not illustrated in the figure). Both small peaks B and C at 18.3 and 15.1 eV correspond to four MOs with bonding F 2p, P 3s, and P 3p character. Thus, these two peaks are representative of P−F bonds in $LiPF_6$. Finally, the massif at 9−13 eV (peaks D and E) can be assigned to a nonbonding MO of dominant F 2p character (lone pairs). For both salts, the good correlation between experimental and simulated spectra proves the validity of the calculation method.

LiTFSI and LiBETI. As for previous salts, Figure 4 shows experimental (a) and calculated (b) spectra of LiTFSI and LiBETI. In the valence spectrum of LiTFSI, nine peaks (A−I) can be considered. The calculation results allow us to assign peaks A, C, and D to MOs of solely F 2s, O 2s, and N 2s dominant character, respectively, with a very low contribution of other AOs in each case. These three peaks have a strong atomic character. Peak B originates from two MOs of S 3s, O 2s, and N 2s character (1) and corresponds to S−O and S−N bonds in the molecule. Peaks E and F originate from three MOs (2 and 3) involving bonding interactions between the S 3p, O 2s, and N 2p AOs, on one hand, and between C 2s and F 2p, on the other hand. For peaks G, H, and I, only selected MOs have been depicted in the figure (4−7) due to the great number of MOs corresponding to these peaks. Peak G can be assigned to MOs of bonding C 2p and F 2p character (4) and corresponds to C−F bonds. Peak H results from several MOs (5 and 6) involving bonding interactions between sulfur and oxygen AOs but also corresponds to nonbonding MOs of dominant F 2p character (fluorine lone pairs). Finally, peak I can be assigned to nonbonding MOs of dominant O 2p and N 2p character (oxygen and nitrogen lone pairs).

Due to the great similarity between LiTFSI and LiBETI, only the MOs of $BETI^-$ that show a significant difference as compared to $TFSI^-$ have been illustrated in Figure 4. The first main difference between both valence spectra is the decrease of peaks B, C, D, and I of LiBETI as compared to LiTFSI. This can be explained by the fact that all of these peaks originate from MOs which are not involving fluorine atoms. Indeed, the main difference between both compounds' formulas is the greater number of fluorine atoms in LiBETI. Thus, peaks corresponding to MOs involving fluorine atoms intensify in comparison to peaks resulting from MOs to which the contribution of fluorine AOs is very low. The second main difference between both spectra concerns peaks E and F in the 17−22 eV energy region. Peak E originates from two MOs of C 2s and F 2p character (1), with a bonding interaction between the C 2s AO. Peak F corresponds to three MOs (2), two of them showing an antibonding interaction between C 2s AOs. Therefore, the difference between both spectra in this energy region originates from the change of the three MOs (2 and 3) in LiTFSI into five MOs (1 and 2) in LiBETI, due to the presence of two additional carbon atoms in the molecule. It results in the splitting of peak E of LiTFSI into both peaks E and F of LiBETI.

In conclusion, the good correlation between the experimental and simulated spectra of all studied salts proves the validity of the calculation method and that each experimental valence spectrum corresponds to a pure salt and not to a mixture of compounds resulting from its degradation in the X-ray beam during XPS experimentation.

3. Application to XPS Study of Electrode/Electrolyte Interfaces. In the following part, the results of this study will be used to characterize electrode/electrolyte interfaces of Li-ion batteries. This concerns graphite negative electrodes taken from usual $LiCoO_2$/graphite cells after a first charge (first electrochemical cycle), when using LiTFSI or LiBETI in the electrolyte. To analyze the surface layer's formation as a function of the battery voltage, we stopped the electrochemical cells at two different potentials: 3.0 V (i.e., at the very beginning of the charge) and 3.8 V (i.e., charge in progress).

Core Peaks. Figure 5 shows C 1s and F 1s core peaks of graphite negative electrodes after charge at 3.0 V (a and b) and 3.8 V (c and d). Corresponding quantitative analysis results are reported in Table 2, as well as those of O 1s, N 1s, S 2p, and Li 1s core peaks (spectra not shown). The C 1s spectrum of sample a (LiTFSI, 3.0 V) shows five components at 284.2,

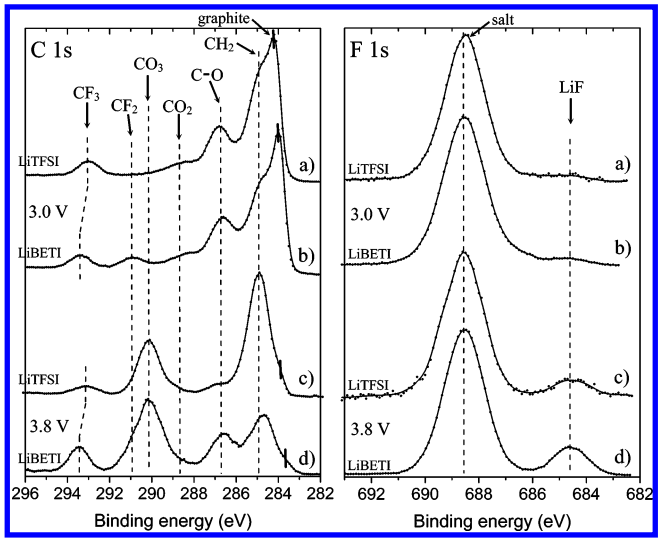

Figure 5. C 1s and F 1s core peaks of the negative carbon electrodes after charge of the battery at 3.0 and 3.8 V when using LiTFSI or LiBETI as lithium salt in the electrolyte.

TABLE 2: Binding Energies (eV) and Atomic Percentages (%) from XPS Core Peaks of the Negative Carbon Electrodes after Charge of the Battery at 3.0 and 3.8 V When Using LiTFSI or LiBETI as the Lithium Salt in the Electrolyte

	3.0 V				3.8 V			
	LiTFSI		LiBETI		LiTFSI		LiBETI	
peak	BE (eV)	%	BE (eV)	%	BE (eV)	%	BE (eV)	%
C 1s	284.2	22	284.0	22	284.0	0.6	283.7	0.4
	284.9	26	284.9	21	285.0	22	284.8	7.1
	286.8	12	286.7	11.5	286.7	2.4	286.7	5.7
	288.5	3	288.5	3.5	288.8	0.9	288.7	0.8
					290.2	9.4	290.1	9
			291.0	2.5			291.0	2.3
	293.1	3.2	293.4	3	293.1	1.3	293.5	2.5
O 1s	531.8	3.1	531.7	3.5	531.8	27	531.8	28
	533.1	12	532.9	11	533.0	7.6	533.2	7
F 1s	684.6	0.4	684.7	0.5	684.6	0.4	684.6	1.7
	688.6	8	688.6	12	688.6	4	688.5	12
N 1s	399.6	2	399.5	2	399.6	0.9	399.5	1.7
S $2p_{3/2}$	167.2	0.3	167.3	0.5	167.4	0.5	167.4	0.8
	169.3	4.5	169.4	3.5	169.4	2	169.4	3
Li 1s	56.0	3.5	55.9	3.5	55.6	21	56.0	18

284.9, 286.8, 288.5, and 293.1 eV, respectively. Except for the peak at 284.9 eV assigned to hydrocarbon contamination, all of these peaks can be attributed to the electrode's constituents. Indeed, the peak at 284.2 eV corresponds to graphite active material, both peaks at 286.8 and 288.5 eV originate from C−O and CO_2 groups in the binder CMC (carboxymethyl cellulose), and the peak at 293.1 eV comes from the residual salt LiTFSI at the surface of the electrode, despite washing it by DMC after opening the electrochemical cell. This spectrum is rather close to that of the starting electrode, except for the presence of the salt. All constituents of the electrode can be detected, and graphite still accounts for 22% of all atoms at the surface. Therefore, we can conclude from this spectrum that the surface layer's formation has barely started at 3.0 V. The same comments about the C 1s spectrum of sample b (LiBETI, 3.0 V) can be made. All peaks of electrode's constituents can be detected, graphite still accounts for 22%, and the main difference with the C 1s spectrum of the starting electrode is the presence of both peaks at 291.0 and 293.4 eV attributed to the salt LiBETI. Actually, taking into account all of the percentages assigned to LiTFSI or LiBETI, the amount of salt in both samples after charge at 3.0 V can be estimated at about 28−30% of all atoms detected at the surface. F 1s spectra of the same samples (a and b) show a first component at 688.6 eV assigned to CF_2 and CF_3 groups of LiTFSI and LiBETI and a very small peak at 684.6 eV attributed to traces of LiF (less than 1%) resulting from a partial degradation of the salt. This weak degradation can also be detected by the presence of a small S 2p peak at 167.2 eV (≈0.3−0.5%).

C 1s spectra of samples after charge at 3.8 V are very different. The spectrum of sample c (LiTFSI) shows, besides the peak at 285.0 eV assigned to hydrocarbon contamination, a very small component at 284.0 eV assigned to graphite (≈0.6%). This strong decrease of the graphite signal shows that the electrode's surface has been covered by a passivation layer. The other main feature is the appearance of a peak at 290.2 eV attributed to CO_3-like carbon atoms. They originate from Li_2CO_3 and/or lithium alkyl carbonate species $ROCO_2Li$. Such carbonate species have been widely described as the main components of surface layers forming on graphite negative electrodes.[3,35,36] Several mechanisms have been reported to explain their formation by electrochemically driven reduction of electrolyte's solvents:

$$\text{DMC}\quad CH_3OCO_2CH_3 + 2e^- + 2Li^+ \rightarrow Li_2CO_3 + C_2H_{6(g)} \tag{3}$$

$$\text{DMC}\quad 2CH_3OCO_2CH_3 + 2e^- + 2Li^+ \rightarrow 2CH_3OCO_2Li + C_2H_{6(g)} \tag{4}$$

$$\text{EC}\quad (CH_2O)_2CO + 2e^- + 2Li^+ \rightarrow Li_2CO_3 + C_2H_{4(g)} \tag{5}$$

$$\text{EC}\quad 2(CH_2O)_2CO + 2e^- + 2Li^+ \rightarrow LiO_2CO{-}CH_2CH_2{-}OCO_2Li + C_2H_{4(g)} \tag{6}$$

However, in $ROCO_2Li$ species, the numbers of carbon atoms bound to three oxygens and bound to one oxygen are the same. Thus, if those species were the main carbonate compounds at the electrode's surface, one should observe two peaks of equal intensity at 290.2 and 286.7 eV, which is not observed in the C 1s spectrum of sample c. We can thus conclude, owing to the peaks' amplitudes, that the main carbon-containing species is Li_2CO_3 in that sample. Besides, we can observe a small peak at 293.1 eV resulting from the presence of LiTFSI salt, despite washing the electrode by the solvent DMC after the electrochemical reaction. Finally, a small component at 288.8 eV attributed to CO_2-like carbon atoms can be noticed, that accounts for less than 1% (the width of this component was constrained in the fit). It appears that this small peak does not come from the binder CMC, because all signals of the electrode's constituents have dramatically decreased due to the covering of the electrode by a passivation layer. Actually, this component could be explained by a small amount of oxalates at the surface. Their formation mechanism has been discussed in a previous work[19] and could be due to solvents' decomposition reactions leading to the formation of CO_2.

The spectrum of sample d (LiBETI, 3.8 V) shows some similarities to that of sample c but also important differences. Hydrocarbon contamination at 284.8 eV can fluctuate from one sample to another and here is weaker than for sample c. In the same way as the previous sample, we can observe a strong decrease of the graphite peak at 283.7 eV (≈0.4%), showing again that the electrode's surface has been covered by a passivation layer. Both peaks related to the salt LiBETI can also be detected at 293.5 and 291.0 eV. However, the main

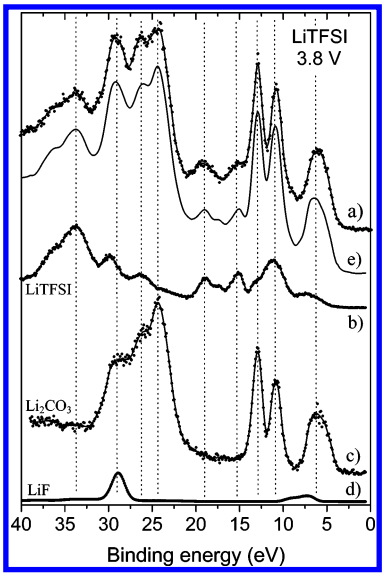

Figure 6. Experimental valence spectra of (a) a carbon electrode after charge of the battery at 3.8 V using LiTSFI salt, (b) LiTSFI, (c) Li_2CO_3, (d) LiF, and (e) a simulation obtained from a summation of spectra b−d.

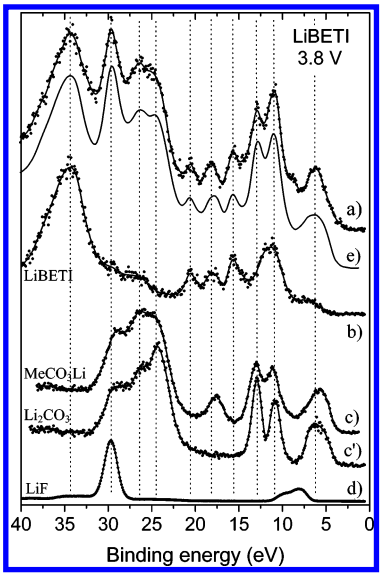

Figure 7. Experimental valence spectra of (a) a carbon electrode after charge of the battery at 3.8 V using LiBETI salt, (b) LiBETI, (c) Li_2CO_3, (c′) CH_3OCO_2Li, (d) LiF, and (e) a simulation obtained from a summation of spectra b, c, c′, and d.

difference between sample d obtained with LiBETI and sample c obtained with LiTFSI concerns the relative intensities of both peaks at 290.1 and 286.7 eV. The shape of spectrum d could be explained by a mixture of about 50% Li_2CO_3 and 50% $ROCO_2Li$. However, previous works have shown that other species in which carbon atoms are in a one-oxygen environment can also be found at the surface of Li-ion electrodes, especially oligomeric species of poly(ethylene oxide) PEO, $(-CH_2-CH_2-O-)_n$ or ROLi species.[19,37,38] The formation of PEO oligomers can be explained by a ring-opening mechanism of the solvent EC, leading to the formation of CO_2 (eq 7). Indeed, it is well-known that the pressure increase occurring in Li-ion batteries using carbonate solvent-based electrolytes upon cycling is partially due to the release of CO_2 gas.

$$\text{EC} \quad n(CH_2O)_2CO \rightarrow (-CH_2-CH_2-O-)_n + nCO_2 \tag{7}$$

Therefore, the relative intensities of peaks at 290.1 and 286.7 eV in sample d can also be due to a mixture of Li_2CO_3 and other species including carbon atoms in a one-oxygen environment, like PEO oligomers $(-CH_2-CH_2-O-)_n$. The sole analysis of C 1s core peaks is thus not sufficient to remove the indetermination about the nature of carbon-containing species at the electrode/electrolyte interface of this sample.

Besides, the F 1s spectra of samples c and d show a first component at 688.6 eV assigned to LiTFSI and LiBETI and a second component at 684.6 eV assigned to LiF. We can notice that the amount of LiF is greater at 3.8 V than at 3.0 V for both salts. Simultaneously, we can observe a slight increase of the S 2p component at 167.4 eV (see Table 2), which confirms a small degradation of the salt upon charge at 3.8 V. In summary, the results of this core peak analysis show that the expected compounds in the surface layer are the lithium salt, LiF, and carbon-containing species including carbonates. However, analysis of the valence spectra will be necessary to clearly identify all compounds.

Valence Spectra. Figure 6 shows the experimental valence spectra of (a) the graphite electrode after charge at 3.8 V with LiTFSI as the lithium salt, (b) LiTFSI, (c) Li_2CO_3, (d) LiF, and a simulated spectrum (e) obtained by a linear combination of reference spectra b−d. The spectrum of sample a displays several recognizable peaks: we can see at 24 eV the narrow maximum of Li_2CO_3 as well as its other characteristic peaks at 13, 11, and 6 eV. We can also recognize the narrow maximum of LiF at 29 eV and a massif at 37−32 eV corresponding to the salt LiTFSI. According to the previous core peak analysis, all of these constituents are expected at the electrode's surface. As we can see in Figure 6, the simulated spectrum e is very close to the experimental spectrum a of the electrode. Therefore, the valence spectrum of this sample appears as the superposition of valence spectra of Li_2CO_3, LiTFSI, and LiF, which shows that the surface layer mainly consists of a mixture of these compounds and confirms the hypothesis made from the core peaks study. Considering the quantitative analysis from core peaks reported in Table 2, this result enables us to propose an approximate composition of the graphite negative electrode's surface (in mol %, excluding hydrocarbon contamination): ≈72−73% of Li_2CO_3, ≈15−16% of LiTFSI, ≈1% of LiF, and ≈0.8% of graphite. The remaining 10% bring together minority species including PEO oligomers $(-CH_2-CH_2-O-)_n$, $ROCO_2Li$, ROLi, and oxalate species.

In the same way, Figure 7 shows the experimental valence spectra of (a) the graphite electrode after charge at 3.8 V with LiBETI as the lithium salt, (b) LiBETI, (c) CH_3OCO_2Li, (c′) Li_2CO_3, (d) LiF, and a simulated spectrum (e) obtained by a linear combination of reference spectra b, c, c′, and d. The spectrum of sample a is more complex than that for the previous sample, but several peaks can also be identified. First, the broad peak at 37−32 eV comes from the salt LiBETI. Then, the narrow peak at 29 eV comes from LiF. Finally, the three peaks at 13, 11, and 6 eV are characteristic of carbonate species. Indeed, valence spectra of Li_2CO_3 and $ROCO_2Li$ species have been described in a previous paper.[20] Spectra c and c′ show two main differences: (1) the narrow maximum of Li_2CO_3 at 24 eV strongly decreases in CH_3OCO_2Li and is replaced by a shoulder, and (2) an additional peak appears at 17−18 eV in CH_3OCO_2Li. In the spectrum of sample a, we clearly can see that the narrow peak at 24 eV has strongly decreased and has been replaced by a shoulder, contrary to the previous electrode (Figure 6). This curve shape enables us to suppose that Li alkyl carbonates species are present, which was one of the possibilities

resulting from the C 1s core peak analysis. This led us to simulate spectrum e by using a mixture of 50% CH_3OCO_2Li (c) and 50% Li_2CO_3 (c′). As we can see in Figure 7, the result of this simulation is very close to the experimental spectrum a of the electrode, which allows us to conclude that the surface layer actually consists of a mixture of Li_2CO_3 and $ROCO_2Li$ species. Indeed, if the surface layer was made up of a mixture of Li_2CO_3 and PEO oligomers, the simulation would not be so close to the experiment, since PEO oligomers have very different valence spectra from those of Li alkyl carbonate species.[19] Note that this exploitation of valence spectra does not allow us to affirm that CH_3OCO_2Li is the only Li alkyl carbonate compound at the surface of the electrode, since Li ethylene dicarbonate $LiO_2CO-CH_2CH_2-OCO_2Li$ would give a similar result. Either Li methyl carbonate or Li ethylene dicarbonate has been already displayed as one of the main constituents of the electrode's surface when using a carbonate-based electrolyte.[19,39] However, our results show that Li_2CO_3 and $ROCO_2Li$-like compounds are undoubtedly the main species at the electrode/electrolyte interface, together with the salts LiBETI and LiF. Then, considering the quantitative analysis from core peaks reported in Table 2, we propose an approximate composition of the graphite negative electrode's surface (in mol %, excluding hydrocarbon contamination): ≈55% of a Li_2CO_3/$ROCO_2Li$ mixture, ≈31% of LiBETI, ≈4% of LiF, and ≈0.4% of graphite, with the remaining 10% being assigned to minority species including PEO oligomers $(-CH_2-CH_2-O-)_n$, ROLi, and oxalate species. As a result, we can conclude that the surface layers of both electrodes have different compositions depending on whether LiTFSI or LiBETI is used in the electrolyte. With LiTFSI, Li_2CO_3 is the main carbon-containing compound formed after charge at 3.8 V, while, with LiBETI, a mixture of Li_2CO_3 and $ROCO_2Li$ species is formed.

Conclusion

In this study, we carried out the experimental XPS valence characterization of four lithium salts used in Li-ion batteries: $LiPF_6$, $LiBF_4$, LiTFSI, and LiBETI. By means of DFT calculations, we could interpret and simulate their valence spectra. We could show that their valence spectra are not affected by a possible degradation in the X-ray beam during XPS recording and thus that they can be exploited as reference valence spectra. Then, by a combined XPS core peaks/valence analysis, we characterized the passivation layers formed at the surface of graphite negative electrodes when LiTFSI or LiBETI is used in the electrolyte. Our conclusions are the following: (1) With each salt, the main interface mechanism upon charge leads to the formation of carbonate species by reduction of the solvents. (2) With LiTFSI, the major carbonate species is Li_2CO_3, while, with LiBETI, a mixture of Li_2CO_3 and Li alkyl carbonates is formed.

Acknowledgment. The authors wish to thank SAFT company for electrode manufacture and financial support.

References and Notes

(1) Xu, Y. *Chem. Rev.* **2004**, *104*, 4303−4418.

(2) Peled, E. *J. Electrochem. Soc.* **1979**, *126*, 2047.

(3) Fong, R.; Von Sacken, U.; Dahn, J. R. *J. Electrochem. Soc.* **1990**, *137*, 2009.

(4) Guyomard, D; Tarascon, J.-M. *J. Electrochem. Soc.* **1993**, *140*, 3071.

(5) Ein-Eli, Y; McDevitt, S. F.; Aurbach, D.; Markovsky, B.; Schechter, A. *J. Electrochem. Soc.* **1997**, *144*, L180.

(6) Besenhard, J. O.; Winter, M.; Yang, J.; Biberacher, W. *J. Power Sources* **1995**, *54*, 228.

(7) Tarascon, J.-M.; Guyomard, D. *Solid State Ionics* **1994**, *69*, 293.

(8) Besenhard, J. O.; Wagner, M. W.; Winter, M.; Jannakoudakis, A. D.; Jannakoudakis, P. D.; Theodoridou, E. *J. Power Sources* **1993**, *44*, 413−420.

(9) Aurbach, D.; Gamolsky, K.; Markovsky, B.; Gofer, Y.; Schmidt, M.; Heider, U. *Electrochim. Acta* **2002**, *47*, 1423−1439.

(10) Herstedt, M.; Rensmo, H.; Siegbahn, H.; Edström, K. *Electrochim. Acta* **2004**, *49*, 2351−2359.

(11) Aurbach, D.; Zinigrad, E.; Cohen, Y.; Teller, H. *Solid State Ionics* **2002**, *148*, 405−416.

(12) Andersson, A. M.; Herstedt, M.; Bishop, A. G.; Edström, K. *Electrochim. Acta* **2002**, *47*, 1885−1898.

(13) Möller, K.-C.; Santner, H. J.; Kern, W.; Yamaguchi, S.; Besenhard, J. O.; Winter, M. *J. Power Sources* **2003**, *119−121*, 561−566.

(14) Hu, Y.; Kong, W.; Wang, Z.; Huang, X.; Chen, L. *Solid State Ionics* **2005**, *176*, 53−56.

(15) Ismail, I.; Noda, A.; Nishimoto A.; Watanabe, M. *Electrochim. Acta* **2001**, *46*, 1595−1603.

(16) Kanamura, K.; Tamura, H.; Shiraishi, S.; Takehara, Z. *J. Electrochem. Soc.* **1995**, *142*, 340−347.

(17) Schechter, A.; Aurbach, D.; Cohen, H. *Langmuir* **1999**, *15*, 3334−3342.

(18) Leroy, S.; Blanchard, F.; Dedryvère, R.; Martinez, H.; Carré, B.; Lemordant, D.; Gonbeau, D. *Surf. Interface Anal.* **2005**, *37*, 773−781.

(19) Dedryvère, R.; Laruelle, S.; Grugeon, S.; Gireaud, L.; Tarascon, J.-M.; Gonbeau, D. *J. Electrochem.* Soc. **2005**, *152*, A689−A696.

(20) Dedryvère, R.; Gireaud, L.; Grugeon, S.; Laruelle, S.; Tarascon, J.-M.; Gonbeau, D. *J. Phys. Chem. B* **2005**, *109*, 15868−15875.

(21) Shirley, D. A. *Phys. Rev. B* **1972**, *5*, 4709.

(22) Scofield, J. H. *J. Electron Spectrosc. Relat. Phenom.* **1976**, *8*, 129−137.

(23) (a) Becke, A. D. *J. Chem. Phys.* **1993**, *98*, 5648. (b) Lee, C.; Yang, W.; Parr, R. G. *Phys. Rev. B* **1988**, *37*, 785.

(24) Frisch, M. J.; Trucks, G. W.; Schlegel, H. B.; Scuseria, G. E.; Robb, M. A.; Cheeseman, J. R.; Zakrzewski, V. G.; Montgomery, J. A., Jr.; Stratmann, R. E.; Burant, J. C.; Dapprich, S.; Millam, J. M.; Daniels, A. D.; Kudin, K. N.; Strain, M. C.; Farkas, O.; Tomasi, J.; Barone, V.; Cossi, M.; Cammi, R.; Mennucci, B.; Pomelli, C.; Adamo, C.; Clifford, S.; Ochterski, J.; Petersson, G. A.; Ayala, P. Y.; Cui, Q.; Morokuma, K.; Malick, D. K.; Rabuck, A. D.; Raghavachari, K.; Foresman, J. B.; Cioslowski, J.; Ortiz, J. V.; Stefanov, B. B.; Liu, G.; Liashenko, A.; Piskorz, P.; Komaromi, I.; Gomperts, R.; Martin, R. L.; Fox, D. J.; Keith, T.; Al-Laham, M. A.; Peng, C. Y.; Nanayakkara, A.; Gonzalez, C.; Challacombe, M.; Gill, P. M. W.; Johnson, B. G.; Chen, W.; Wong, M. W.; Andres, J. L.; Head-Gordon, M.; Replogle, E. S.; Pople, J. A. *Gaussian 98*, revision A.7; Gaussian, Inc.: Pittsburgh, PA, 1998.

(25) Gelius, U. In *Electron spectroscopy*; Shirley, D. A., Ed.; North-Holland: Amsterdam, The Netherlands, 1972; p 311.

(26) Gelius, U. *J. Electron Spectrosc. Relat. Phenom.* **1974**, *5*, 985.

(27) Huang, J. T. J.; Rabalais, J. W. In *Electron Spectroscopy*: *theory, techniques and applications*; Brundle, C. R., Baker, A. D., Eds.; Academic Press: New York, 1978.

(28) Endo, K.; Kaneda, Y.; Okada, H.; Chong, D. P.; Duffy, P. *J. Phys. Chem.* **1996**, *100*, 19455−19460.

(29) Brena, B.; Zhuang, G. V.; Augustsson, A.; Liu, G.; Nordgren, J.; Guo, J.-H.; Ross, P. N.; Luo, Y. *J. Phys. Chem. B* **2005**, *109*, 7907−7914.

(30) Andersson, A. M.; Abraham, D. P.; Haasch, R.; McLaren, S.; Liu, J.; Amine, K. *J. Electrochem. Soc.* **2002**, *149*, A1358−A1369.

(31) Arnaud, R.; Benrabah, D.; Sanchez, J.-Y. *J. Phys. Chem.* **1996**, *100*, 10882−10891.

(32) Rey, I.; Johansson, P.; Lindgren, J.; Lassègues, J. C.; Grondin, J.; Servant, L. *J. Phys. Chem. A* **1998**, *102*, 3249−3258.

(33) Johansson, P.; Gejji, S. P.; Tegenfeldt, J.; Lindgren, J. *Electrochim. Acta* **1998**, *43*, 1375−1379.

(34) Johansson, P.; Tegenfeldt, J.; Lindgren, J. *J. Phys. Chem. A* **2000**, *104*, 954−961.

(35) Aurbach, D.; Daroux, M. L.; Faguy, P. W.; Yeager, E. *J. Electrochem. Soc.* **1987**, *134*, 1611−1620.

(36) Aurbach, D.; Ein-Eli, Y.; Markovsky, B.; Zaban, A.; Luski, S.; Carmeli, Y.; Yamin, H. *J. Electrochem. Soc.* **1995**, *142*, 2882−2889.

(37) Ogumi, Z.; Sano, A.; Inaba, M.; Abe, T. *J. Power Sources* **2001**, *97−98*, 156−158.

(38) Laruelle, S.; Pilard, S.; Guenot, P.; Grugeon, S.; Tarascon, J.-M. *J. Electrochem. Soc.* **2004**, *151*, 1202−1209.

(39) Zhuang, G. V.; Xu, K.; Yang, H.; Jow, T. R.; Ross, P. N., Jr. *J. Phys. Chem. B* **2005**, *109*, 17567−17573.